Dalton Transactions

Accepted Manuscript

ROYAL SOCIETY OF CHEMISTRY

www.rsc.org/dalton

Four linear Cu^{II}_3 subunit-based coordination polymers with various inter-subunit connections, spin ground-states and intra-/inter-subunit magnetic couplings

En-Cui Yang,[a, *] Zhong-Yi Liu,[a] Si-Hang Chen,[a] Yan-Hong Su,[a] Yan-Yan Zhang[a] and Xiao-Jun Zhao[a, b, *]

[a] *Key Laboratory of Inorganic-Organic Hybrid Functional Material Chemistry*, *Ministry of Education*, *Tianjin Key Laboratory of Structure and Performance for Functional Molecules*, *College of Chemistry*, *Tianjin Normal University*, *Tianjin 300387*, *P. R. China. E-mail*: encui_yang@163.com, xiaojun_zhao15@163.com; *Fax: +86-22-23766556*

[b] *Collaborative Innovation Center of Chemical Science and Engineering (Tianjin), Tianjin 300071, P. R. China*

† Electronic supplementary information (ESI) available: PXRD patterns, selected bond distances and angles, and X-ray crystallographic files in CIF format for **1**–**4**, additional figures for **1**–**3**, TG curves for **1**, **2** and **4**, magnetic diagrams for **1** and **4**. CCDC 1036044, 1007286, 1027763 and 1007288 for **1**–**4**. For ESI and crystallographic data in CIF or other electronic format see DOI:10.1039/

To *Dalton Trans.* (*Research Paper*)

Four new 4-amino-1,2,4-triazole (atr)-based coordination polymers, $\{[Cu_2(atr)(H_2O)(\mu\text{-}OH)_2(pa)]\cdot H_2O\}_n$ (**1**), $\{[Cu_3(atr)_2(H_2O)_2(\mu\text{-}OH)_2(npa)_2]\cdot 2H_2O\}_n$ (**2**), $\{[Cu_3(atr)_5(dca)(\mu\text{-}OH)(ClO_4)_2](ClO_4)_2\}_n$ (**3**) and $\{[Cu_3(atr)_2(H_2O)(\mu_3\text{-}OH)(\mu\text{-}OH)_2(spa)]\cdot 1.5H_2O\}_n$ (**4**) (pa^{2-} = phthalate, npa^{2-} = 3-nitrophthalate, dca^- = dicyanamide and spa^{3-} = 4-sulfophthalate), were successfully obtained by varying carboxylate- and cyanide-modified magnetic bridges. Structural determinations reveal that the former three samples are bent one-dimensional chains constructed from linear Cu^{II}_3 subunits and different inter-subunit connections. In **1**, linear $\{Cu_3(\mu\text{-N1,N2-atr})_2(\mu\text{-}OH)_2\}^{4+}$ and $\{Cu_3(\mu\text{-}COO)_2(\mu\text{-}OH)_2\}^{4+}$ subunits are alternately connected in a sharing-vertex manner to give a ferrimagnetic S = 1/2 spin ground-state. While linear $\{Cu_3(\mu\text{-N1,N2-atr})_2(\mu\text{-}OH)_2\}^{4+}$ building block of **2** is repeatedly bridged by pairs of single-atom bridging carboxylate group of npa^{2-} ligand to lead to a paramagnetic S =1/2 spin ground-state. By contrast, each linear $\{Cu_3(\mu\text{-N1,N2-atr})_4\}^{6+}$ core in **3** is periodically propagated by four-fold heterobridges (μ-OH^-, μ-ClO_4^-, μ-N1,N2-atr and μ-dca^-) to generate an overall diamagnetic S = 0 spin ground-state. Complex **4** is a three-dimensional pillared-layer framework composed of linear $\{Cu_3(\mu\text{-N1,N2-atr})_2(\mu\text{-}OH)_2\}^{4+}$-based layers and ditopic spa^{3-} connectors, which exhibits a ferrimagnetic S =1/2 spin ground-state and a metamagnetic transition resulting from the competition between the weak interchain/interlayer antiferromagnetic interaction and the enhanced external magnetic field. Additionally, different intra- and inter-subunit magnetic strength are observed in **1**–**4** with the coupling constants $182 < -J_{intra} < 43$ and $-127 < J_{inter} < 51.2$ cm^{-1}. These interesting magnetostructural results are significant and helpful for the cyclic polyazolate-based magnetic materials.

Introduction

Molecule-based magnetic materials that constructed from paramagnetic metal ion and short organic mediator have recently received intense interest due to their intriguing structures,[1] potential applications in information storage and spintronic devices,[2–4] as well as the deep understanding on the fundamental magnetostructural relationships.[5–6] Synthetically, two important factors, spin carrier and short magnetic mediator, should be carefully considered during the self-assembly process of the targeted entities because of the following considerations. On one hand, magnetic anisotropy, spin-orbit coupling and the unpaired *d*/*f* electron number of the spin carrier can significantly control the slow relaxation of the magnetization,[7] magnetocaloric effect[8] as well as spin-crossover behavior.[9] On the other hand, short organic mediator bearing various coordinative functional groups can essentially direct the sign and strength of the exchange coupling between the ligand and metal ion through the binding mode, conformation, bridging angle and other geometric parameters.[5–6] Especially, the magnetic anisotropy of the paramagnetic metal ion can be fine-tuned via the ligand-field environments. Thus, as compared to the spin carrier, the magnetic mediator play more important roles to some different extent for the structures and resulting magnetic behaviors of the target complexes. Therefore, tremendous efforts have been recently paid on the design and choice of single or mixed mediators. Coplanar five-membered N-heterocyclic ligands with two or more N donors, such as isomeric imidazole and pyrazole, 1,2,3- and 1,2,4-triazole, as well as tetrazole and their diverse derivatives, can provide two different superexchange pathways (–NN– and –NCN–) by selective coordination with paramagnetic ion (μ-N1, N2-, μ-N1, N3-, μ_3-N1, N2, N3-, μ_3-N1, N2, N4- as well as μ_4-N1, N2, N3, N4-) favorable for antiferromagnetic coupling and asymmetric magnetic exchange.[10] Moreover, crystallographically, the both pathways can further chelate synergically with other single- or double-atom short bridges to generate sterically stable five-membered metallocyclic subunits,[11] which can act as fundamentally structural subunits to take part in the subsequent self-assembly processes. Thus, the polyazole-based magnetic

samples incorporated with linear azido-,[12–13] diatomic hydroxyl group, angular carboxylate[14] as well as pseudo halogen bridges[15] have been extensively investigated, which can serve as intriguingly high-dimensional ordering magnets, single-chain magnets as well as single molecule magnets.[16]

As continuous investigations on the magnetostructural relationships of the mixed heterobridges-based molecular-based magnetic materials, herein, cyclic 4-amino-1,2,4-triazole (atr) and bent carboxylate or diatomic cyanide modified coligand were selected to self-assembly with anisotropic Cu^{II} ion. In this context, we reported the synthesis, structure and magnetism of the resulting four coordination polymers with linear Cu^{II}_3 motifs and different dimensionalities. These significant results are helpful and suggestive for cyclic triazole-based magnetic materials.

Experimental

Materials and general methods

All the initial reagents were commercially purchased (atr, phthalic acid (H_2pa), 3-nitrophthalic acid (H_2npa), $NaN(CN)_2$ and 4-sulfophthalic acid (H_3spa) were from Acros, and other analytical-grade reagents were from Tianjin chemical reagent factory) and used without further purification. Doubly deionized water was used for the conventional synthesis. Elemental analyses for C, H and N were carried out with a CE-440 (Leeman Labs) analyzer. Fourier transform (FT) IR spectra (KBr pellets) were taken on an Avatar-370 (Nicolet) spectrometer in the range 4000–400 cm^{-1}. Thermogravimetric analysis (TGA) experiments were performed on a Shimadzu simultaneous DTG-60A compositional analysis instrument from room temperature to 800 ^oC in a N_2 atmosphere at a heating rate of 5 ^oC min^{-1}. Powder X-ray diffraction (PXRD) patterns were obtained using a Bruker D8 ADVANCE diffractometer at 40 kV and 40 mA for Cu-*K*α radiation (λ = 1.5406 Å), with a scan speed of 0.1 s per step and a step size of 0.01 ^{o} in 2θ. The simulated PXRD patterns were calculated using single-crystal X-ray diffraction data and processed by the free Mercury v1.4 program provided by the Cambridge Crystallographic

Data Center. Magnetic susceptibilities were acquired on a Quantum Design (SQUID) magnetometer MPMS-XL-7 with phase-pure crystalline samples. The diamagnetic corrections were calculated using Pascal's constants, and an experimental correction for the sample holder was also applied.

Preparations of complexes 1–4

{[Cu_2(atr)(H_2O)(μ-OH)$_2$(pa)]·H_2O}$_n$ (1). An ethanol solution (5.0 mL, pH = 6 adjusted by LiOH solution) of H_2pa (16.6 mg, 0.1 mmol) was carefully layered onto a buffer layer of ethyl acetate (3.0 mL) in a test tube, below which an aqueous solution (5.0 mL) containing atr (16.8 mg, 0.2 mmol) and $Cu(OAc)_2{\cdot}H_2O$ (19.9 mg, 0.1 mmol) was placed. Blue block-shaped crystals of **1** suitable for X-ray diffraction were generated in a week upon slow evaporation of the solvents at room temperature. Yield: 36% based on Cu^{II} salt. Anal. Calc. for $Cu_2C_{10}H_{14}N_4O_8$: C, 26.97; H, 3.17; N, 12.58%. Found: C, 26.94; H, 3.19; N, 12.55%. IR (KBr, cm^{-1}): 3437(br), 1636(s), 1603(s), 1578(s), 1555(s), 1406(s), 1084(m), 1048(m),1013(m), 770(w), 617(w), 540(w).

{[Cu_3(atr)$_2$(H_2O)$_2$(μ-OH)$_2$(npa)$_2$]·2H_2O}$_n$ (2). $Cu(NO_3)_2{\cdot}6H_2O$ (24.1 mg, 0.1 mmol), atr (16.8 mg, 0.2 mmol), H_2npa (21.1 mg, 0.1 mmol), doubly deionized water (8.0 mL) and aqueous LiOH solution (0.2 mol·L^{-1}, 1.0 mL) were sealed in a Teflon-lined reactor (23.0 mL) and heated at 100 °C for 168 hours. After the mixture was cooled to room temperature at a rate of 1.6 °C·h^{-1}, blue block-shaped crystals suitable for X-ray analysis were obtained directly, washed with ethanol and dried in air. Yield: 49% based on Cu^{II} salt. Anal. Calc. for $Cu_{1.5}C_{10}H_{12}N_5O_9$: C, 27.20; H, 2.74; N, 15.86%. Found: C, 27.24; H, 2.78; N, 15.81%. IR (KBr, cm^{-1}): 3597(w), 3451(br), 3337(w), 3166(w), 3107(w), 3061(w), 3017(w), 1613(s), 1603(s), 1555(s), 1527(s), 1449(s), 1381(s), 1351(s), 1258(m), 1076(m), 1058(m), 1020(m), 998(w), 923(m), 827(w), 790(w), 763(w), 710(m), 622(m), 574(w), 545(w).

{[Cu_3(atr)$_5$(dca)(μ-OH)(ClO_4)$_2$](ClO_4)$_2$}$_n$ (3). To an ethanol solution (5.0 mL) containing atr (0.2 mmol, 16.8 mg) and $NaN(CN)_2$ (0.1 mmol, 8.9 mg) was slowly added an aqueous solution (5.0 mL) of $Cu(ClO_4)_2{\cdot}6H_2O$ (0.2 mmol, 72.2 mg) with constant stirring. The resulting mixture was filtered after further stirring for half an hour.

Blue block-shaped crystals suitable for X-ray diffraction were grown by slow evaporation of the filtrate within seven days. Yield: 56% based on atr. Anal. Calc. for $C_{12}H_{21}Cl_4Cu_3N_{23}O_{17}$: C, 13.20; H, 1.94; N, 29.50%. Found: C, 13.15; H, 2.00; N, 29.40%. FT-IR (KBr, cm^{-1}): 3550(s), 3471(s), 3415(br) 3231(w), 2287(m), 2218(m), 2146(s), 2026(m), 1635(s), 1618(s), 1548(m), 1408(w), 1347(w), 1320(w), 1092(s), 927(w), 881(w), 622(s), 529(w), 463(w).

$\{[Cu_3(atr)_2(H_2O)(\mu_3\text{-}OH)(\mu\text{-}OH)_2(spa)]\cdot 1.5H_2O\}_n$ (4). Atr (16.8 mg, 0.2 mmol), $Cu(OAc)_2\cdot H_2O$ (60.0 mg, 0.3 mmol), triethylamine (40.4 mg, 0.4 mmol) and H_3spa (26.8 mg, 0.1 mmol) were dissolved in doubly deionized water (8.0 mL). The resulting mixture was then transferred into a parr Teflon-lined stainless steel vessel (23.0 mL) and heated at 100 °C for 96 hours under autogenous pressure. After the mixture was cooled to room temperature at a rate of 3.3 °C h^{-1}, blue block-shaped crystals suitable for X-ray analysis were generated directly, washed with water and dried in air. Yield: 40% based on Cu^{II} salt. Anal. Calc. for $C_{24}H_{38}Cu_6N_{16}O_{25}S_2$: C, 20.65; H, 2.74; N, 16.05%. Found: C, 20.66; H, 2.74; N, 16.04%. FT-IR (KBr, cm^{-1}): 3547(s), 3474(s), 3411(s), 3237(w), 1638(s), 1616(s), 1398(s), 1363(s), 1211(w), 1192(w), 1179(w), 1159(w), 1125(w), 1078(w), 1033(m), 978(w), 887(w), 846(w), 792(w), 748 (w), 621(m), 479(w).

X-ray data collection and structure determinations

Diffraction intensities for **1**–**4** were collected on a Bruker APEX-II QUAZAR diffractometer equipped with a graphite-monochromated Mo-*K*α radiation with a radiation wavelength of 0.71073 Å by using the φ-ω scan technique at 296 (for **1**, **2** and **4**) and 173 K (for **3**). There was no evidence of crystal decay during data collection. Semiempirical multi-scan absorption corrections were applied by SADABS [17] and the program SAINT [18] was used for the integration of the diffraction profiles. The structures were solved by direct methods and refined with the full-matrix least-squares technique using the SHELXS-97 and SHELXL-97 programs.[19] Anisotropic thermal parameters were assigned to all non-H atoms. The organic hydrogen atoms were geometrically generated; the H

atoms of the water molecule were located from difference maps and refined with isotropic temperature factors. Nitro group (N5, O5 and O6) and lattice water molecule (O9) in **2** were varied between two positions with the site occupancies assigned to 0.486 (for N5, O5 and O6) and 0.514 (for N5′, O5′ and O6′), as well as 0.715 (for O9) and 0.285 (for O9′), respectively. Free perchlorate anion in **3** was varied between two different positions with the site occupancy of 0.482 and 0.518. The site occupancy of the co-crystallized water molecules in **4** (O12, O13 and O14) is 0.5, 0.5, and 0.5. No hydrogen atom for splitting water molecule was located. The crystallographic data for **1**–**4** were given in Table 1.

/insert Table 1/

Results and discussion

Syntheses and IR spectra

Three different synthetic approaches (liquid-phase diffusion for **1**, hydrothermal synthesis for **2** and **4** as well as solvent evaporation method for **3**) were applied to obtain the four atr-based magnetic entities with COO^--/CN^--modified coligands. The pH value of the carboxylate-involved reaction systems was specially adjusted by inorganic (LiOH) or organic bases (triethylamine). In the IR spectra, strong and broad bands centered at 3414–3474 cm^{-1} together with several weak absorptions above 3231 cm^{-1} for the N–H and O–H stretching vibrations indicate the presence of the exocyclic amino group of atr, water and/or hydroxyl group in **1**–**4**. An absence of a strong band at ca. 1700 cm^{-1} in **1**, **2** and **4** reveals the deprotonation of the carboxylic group, and the corresponding stretching vibrations locate at 1636–1351 cm^{-1}. The characteristic absorptions for the CN^- (2287–2026 cm^{-1})[20] and ClO_4^- (1092 and 623 cm^{-1}) of **3** as well as the sulfonato group of **4** (1211–1115 and 621 cm^{-1}) are also observed.

Crystal structures of 1–4

$\{[Cu_2(atr)(H_2O)(\mu\text{-}OH)_2(pa)]\cdot H_2O\}_n$ (1). Single-crystal X-ray diffraction analysis reveals that **1** crystallizes in

the triclinic $P\bar{1}$ space group, displaying a bent chain with two linear Cu^{II}_3 subunits alternately extended by sharing the same metal sites. The asymmetric unit of **1** contains three unique Cu^{II} ions with Cu2 and Cu3 located at special positions, one neutral μ-N1, N2-atr molecule, two bridging μ-OH^- groups, one doubly deprotonated pa^{2-} ligand as well as two water molecules in coordinated and free forms. Located at a general position, the unique Cu1 ion is in slightly distorted NO_4 square-pyramidal coordination environments (Fig. 1a) with Addison parameter $\tau = 0.1$. The Addison parameter τ is defined as an index of trigonality ($\tau = 1$) and square-pyramid ($\tau = 0$).[21] The apical site of the Cu1 ion is occupied by one aqua ligand and the NO_3 basal plane is generated by one triazolyl moiety from a neutral atr ligand, two bridging μ-OH^- groups and one carboxylate group of pa^{2-} anion. The apical $Cu–O_{aqua}$ bond length is considerably longer than those in the basal plane (see Table S1). Located at different inversion centers, the other two Cu^{II} ions are in irregular square-planar coordination geometries (O_2N_2 for Cu2 and O_4 for Cu3) fulfilled by pairs of μ-OH^- and μ-atr/μ-COO^- of pa^{2-} ligands. The bond lengths around the Cu2 and Cu3 ions (Table S1) are comparable to those previously reported values in triazolyl- and carboxylate-based metal complexes.[22]

/insert Figure 1/

As shown in Fig. 1b, the central Cu3 ion connects with two centrosymmetric Cu1 and Cu1A ions (A = $-x$, $1-y$, $2-z$) through one μ-OH^- and one μ-*syn*, *syn*-COO^- of pa^{2-} ligand, leading to a strictly linear Cu^{II}_3 subunit with the intermetallic separation of 3.2277(12) Å. Analogously, the central Cu2 ion also aggregates two centrosymmetric Cu1 and Cu1B ions (B = $-x$, $-y$, $1-z$) by one μ-OH^- and one μ-N1, N2-atr ligand to generate another linear Cu^{II}_3 subunit with the intermetallic separation of 3.4102(1) Å. Two unique Cu^{II}_3 subunits are alternately extended by sharing the exterior Cu1 ions to lead to an infinite *zigzag* chain (Fig. 1b).

Adjacent chains of **1** interact with each other by non-covalent O–H···N and N–H···O interactions between the coordinated water molecule and exocyclic amino group of atr ligand as well as between the exocyclic amino

group of atr ligand and non-coordinated carboxylate group of pa^{2-} anion, generating an overall three-dimensional (3D) supramolecular array of **1** (Table S5 and Fig. S1 in the ESI†). The nearest interchain $Cu^{II}\cdots Cu^{II}$ distance (10.5 Å) is almost beyond the effectively magnetic interacting range. Thus, **1** can behave as an isolate one-dimensional (1D) magnetic chain with negligible interchain superexchange coupling.

$\{[Cu_3(atr)_2(H_2O)_2(\mu\text{-}OH)_2(npa)_2]\cdot 2H_2O\}_n$ (2). Complex **2** exhibits a linear $\{Cu_3(\mu\text{-}N1,N2\text{-}atr)_2(\mu\text{-}OH)_2\}^{4+}$ subunit-based 1D *zigzag* chain propagated by pairs of single-atom bridging carboxylate group of npa^{2-} linkers. There are one and a half Cu^{II} ions, one neutral μ-N1,N2-atr molecule, one μ-OH^- group, one doubly deprotonated npa^{2-} ligand and two water molecules in coordinated and free forms in the asymmetric unit. The centrosymmetric Cu1 ion is in a square-planar N_2O_2 donor set completed by two μ-N1, N2-atr and two μ-OH^- groups (Fig. 2a). Lying at a general position, the Cu2 site is in a slightly distorted square-pyramid ($\tau = 0.23$) with the basal plane completed by one triazolyl N and three O donors from a μ-N1, N2-atr, μ-OH^- group, carboxylate group of npa^{2-} anion and coordinated water molecule. The apical site of Cu2 ion is occupied by one carboxylate O atom from another npa^{2-} anion with the apical Cu–O bond length considerably longer than those in the basal planes (see Table S2).

/insert Figure 2/

The central Cu1 ion links two centrosymmetric Cu2 and Cu2A sites by two μ-OH^- and two μ-N1, N2-atr ligands, leading to a linear Cu^{II}_3 subunit with Cu1···Cu2 separation of 3.4044(5) Å (Fig. 2b). Adjacent Cu^{II}_3 subunits of **2** are periodically connected by pairs of single-atom bridging carboxylate group of npa^{2-} ligand, leading to an infinitely bent chain running along the crystallographic *b*-axis with the intersubunit Cu2···Cu2 separation of 3.4258(6) Å.

Adjacent chains of **2** interacts with each other through weak N–H···O and O–H···O hydrogen-bonding interactions (Table S5 in the ESI†), generating a two-dimensional (2D) supramolecular layer with the nearest

interchain intermetallic separation of ca. 7.5599(5) Å (Fig. S2 in the ESI†). Analogous to **1**, complex **2** can also be considered as a magnetically isolated chain due to the longer interchain intermetallic distance.

{[Cu_3(atr)$_5$(dca)(μ-OH)(ClO_4)$_2$](ClO_4)$_2$}$_n$ (3). Complex **3** crystallizes in the orthorhombic *Pnma* space group, exhibiting a bent chain with linear $\{Cu_3(atr)_4\}^{6+}$ subunits propagated by four-fold mirror-symmetric heterobridges ($\mu_{1,1,5,5}$-dca^-, μ-N1,N2-atr, μ-OH^- and μ-ClO_4^-). The asymmetric unit of **3** consists of one and a half unique Cu^{II} atoms, two and a half neutral atr ligands, half a $\mu_{1,1,5,5}$-dca^- anion, half a μ-OH^- group and two ClO_4^- anions in coordinated and free forms. Located at a general position, the Cu1 ion is in a N_4O_2 donor set completed by three separate triazolyl groups, one dca^- anion, one ClO_4^- and one μ-OH^- group (Fig. 3a), adopting an distorted octahedral coordination geometry. By contrast, the centrosymmetric Cu2 site is equatorially surrounded by four triazolyl N atoms and axially occupied by two dca^- coligands, exhibiting an axially elongated octahedral coordination geometry with the equatorial Cu–N distances shorter by 0.4 Å than those in axial positions (Table S3 in the ESI†).

/insert Figure 3/

The central Cu2 ion aggregates two centrosymmetric Cu1 and Cu1A ions through two pairs of unique μ-N1,N2-atr ligands to generate a linear Cu^{II}_3 subunit with the Cu1···Cu2 separation of 3.4807(10) Å (Fig. 3b). The linear Cu^{II}_3 subunits of **3** are further extended by mixed $\mu_{1,1,5,5}$-dca^-, μ-ClO_4^-, μ-N1,N2-atr as well as μ-OH^- heterobridges to give a 1D *zigzag* chain running along the crystallographic *b*-axis with the inter-subunit intermetallic separation of 3.3448(13) Å. Notably, the four heterobridges that connect the adjacent Cu^{II}_3 subunit contain a mirror symmetry with Cl (from μ-ClO_4^-), O (from μ-OH^- group) and two N (from μ_4-dca^- and μ-atr) atoms passing through the mirror. Each chain of **3** connects with each other through the non-covalent N–H···N interactions produced by the amino group of atr ligand, leading to a 3D supramolecular network with the nearest interchain Cu^{II}···Cu^{II} separation of ca. 9.5 Å (Table S5 and Fig. S3 in the ESI†).

{[Cu_3(atr)$_2$(H_2O)(μ_3-OH)(μ-OH)$_2$(spa)]·1.5H_2O}$_n$ (4). Different from the chain-like motifs of **1**–**3**, complex **4** exhibits a 3D pillared-layer framework composed of approximately linear Cu^{II}_3 subunits, pairs of μ_3-OH^- groups that connect the separate Cu^{II}_3 into wave-like layer and ditopic spa^{3-} pillars. The asymmetric unit of **4** consists of three crystallographically independent Cu^{II} ions, two μ-N1,N2-atr, one triply deprotonated spa^{3-} anion, three bridging hydroxyl groups, one bound as well as one and a half disordered lattice water molecules. All the unique Cu^{II} ions in **4** are in the slightly distorted square-pyramidal surroundings with τ = 0.08, 0.05 and 0.13, respectively (Fig. 4a). The basal planes of the metal coordination spheres are respectively generated by NO_3 (for Cu1 and Cu2) and N_2O_2 donor sets (for Cu3) coming from the triazolyl moiety of atr ligand, bridging carboxylate and/or hydroxyl groups. The apical positions are respectively filled by μ_3-OH^- group, terminal aqua and sulfonato moiety of spa^{3-} ligand. The apical Cu−O bond lengths are considerable longer by 0.38–0.60 Å than those in the basal plane (Table S4 in the ESI†).

/insert Figure 4/

The central Cu3 ion connects with two unique Cu1 and Cu2 ions by two μ-OH^- groups and two μ-N1, N2-atr molecules, generating an approximately linear $\{Cu_3(atr)_2(\mu\text{-}OH)_2\}^{4+}$ subunit with the intermetallic distance of 3.3951(11) and 3.3809(11) Å for Cu3···Cu1 and Cu3···Cu2. The adjacent Cu^{II}_3 subunits are further extended by mixed μ_3-OH^- group and μ-*syn*, *syn*-COO^- of spa^{3-} ligand, giving rise to a linear Cu^{II}_3 subunit-based wave-like 2D layer with the nearest interchain separation of 3.2805(13) Å (Fig. 4b). The adjacent layers of **4** are further pillared by the sulfonato group of the sip^{3-} binding to the Cu^{II} ions from the adjacent layers, leading to a pillared-layer framework with the nearest interlayer Cu^{II}···Cu^{II} separation of 9.1669(2) Å (Fig. 4c).

TGA and PXRD analyses of 1–4

The structural consistency and phase purity of the bulk products of **1**–**4** were evidenced by the well matched experimental and computer-simulated PXRD patterns (Fig. S4–S7 in the ESI†). TGA experiments were conducted

to explore the compositional stability of **1**, **2** and **4** (Fig. S8 in the ESI†), in which **3** was not performed due to the presence of the potentially explosive perchlorate anion. The first weight-loss stage between room temperature and 146 °C for **1** was due to the loss of lattice and coordinated water molecules (obsd 8.7%; calcd 8.1%). The polymeric chain of **1** was continuously broken down upon further heating. Free water molecule in **2** was removed between room temperature and 124 °C (obsd 4.3%; calcd 4.0%). The 1D chain of **2** began to broken above 180 °C. The hydroxyl groups, coordinated and lattice water molecules in **4** were released between room temperature and 120 °C. The 3D framework of **4** began to collapse at 196 °C (obsd 10.0%; calcd 13.8%). The weight-loss processes of the three samples were not entirely finished even at 800 °C, suggesting an incomplete decomposition of the mixed ligands.

Magnetic properties of 1–4

Variable-temperature (2.0–300 K) magnetic susceptibilities of the polycrystalline samples of **1–4** were measured under an applied field of 2.0 kOe. As shown in Fig 5a, the $\chi_M T$ value for each dimeric unit of **1** is 0.69 cm^3 K mol^{-1} at 300 K, which is slightly lower than the spin-only value (0.75 cm^3 K mol^{-1}) expected for two magnetically uncoupled Cu^{II} ions with $S = 1/2$ and $g = 2.0$. The $\chi_M T$ product of **1** slightly decreases with the decreasing temperature and reaches a value of 0.62 cm^3 K mol^{-1} at 130 K, suggesting dominate antiferromagnetic couplings occur in the extended chain of **1**. Upon further cooling, the $\chi_M T$ value increases quickly and gets to a value of 2.60 cm^3 K mol^{-1} at 2.0 K. The abrupt rise of the $\chi_M T$ at low temperature implies the inter-subunit ferromagnetic interactions. From the viewpoint of the magnetostructural relationships, the superexchange couplings of **1** are mediated by alternating μ-N1,N2-atr and μ-OH^- as well as μ-*syn*, *syn*-COO^- and μ-OH^- heterobridges. Unfortunately, no exactly magnetic mode can be presently used to fit the magnetic data of **1** due to the presence of the pairs of alternating heterobridges. A previously known fact that a closed 12-membered metallomacrocycle (Fig. S9 in the ESI†) can describe satisfactorily the magnetic behavior of such an extended chain with the spin

Hamiltonian, $\boldsymbol{H} = -J_1(\boldsymbol{S_1S_2}+\boldsymbol{S_2S_3}+\boldsymbol{S_5S_6}+\boldsymbol{S_6S_7}+\boldsymbol{S_9S_{10}}+\boldsymbol{S_{10}S_{11}})-J_2(\boldsymbol{S_3S_4}+\boldsymbol{S_4S_5}+\boldsymbol{S_7S_8}+\boldsymbol{S_8S_9}+\boldsymbol{S_{11}S_{12}}+\boldsymbol{S_{12}S_1})$,[23] in which $\boldsymbol{S_1}$–$\boldsymbol{S_{12}}$ are the spin operators of Cu1–Cu12, J_1 and J_2 are used to describe the coupling constants transferred by two different types of heterobridges. The least-square fit of the magnetic data of **1** above 40.0 K by the MAGPACK suite[24] leads to g = 2.15, J_1 = –182 cm^{-1} and J_2 = 51.2 cm^{-1} with agreement factor $R = \Sigma[(\chi_M T)_{obsd}-(\chi_M T)_{calcd}]^2/\Sigma[(\chi_M T)_{obsd}]^2 = 5.4\times10^{-4}$. Apparently, the big $-J_1$ value should be ascribed to the antiferromagnetic coupling mediated by the mixed μ-OH$^-$ and μ-N1, N2-atr heterobridges, which can be frequently observed in the Cu^{II}-containing complexes with same magnetic bridges.[25] By contrast, the J_2 value confirms the moderate ferromagnetic interaction transferred by the μ-*syn*, *syn*-COO$^-$ and μ-OH$^-$ mediators due to the orbital countercomplementarity.[23, 26]

/insert Figure 5/

The isothermal magnetization of **1** measured at 2.0 K (Fig. 5b) exhibits an initially quick increase at the field lowered than 30 kOe and a slight rise up to 2.08 $N\beta$ at 70 kOe. The magnetization at the highest field confirms a ferrimagnetic S = 1/2 ground-state for each Cu$^{II}_2$ unit of **1** in a double vertex-sharing Cu$^{II}_3$ arrangement.

The $\chi_M T$ product for per Cu$^{II}_3$ subunit of **2** at 300 K (0.69 cm^3 K mol^{-1}) is much lower than the spin-only value (1.12 cm^3 K mol^{-1}) for three magnetically uncoupled Cu^{II} ions with S = 1/2 and g = 2.0, indicating that strong antiferromagnetic interactions dominate among the adjacent spin carriers of **2** even at room temperature. Upon cooling, the $\chi_M T$ product shows a slow decrease and is down to a value of 0.44 cm^3 K mol^{-1} at 2.0 K, revealing a paramagnetic S =1/2 spin ground-state of **2**. The superexchange couplings of the centrosymmetric Cu$^{II}_3$ subunit-based chain of **2** occur between the adjacent Cu^{II} ions mediated by different heterobridges (μ-OH$^-$ and μ-N1,N2-atr for Cu1 and Cu2, as well as a pair of single-atom carboxylate homobridges for two adjacent Cu2 ions), which can be treated as an alternating uniform 1D Heisenberg chain with classical spins.[27–29] The molar susceptibilities of **2** can be treated by the following Eqs. (1)–(4), in which J_1 and J_2 are respectively corresponding

to the intra- and inter-subunit coupling constants, N, g, β, and k have their usual meanings, and S_t is the effective spin of the linear Cu^{II}_3 subunit.

$$\chi_{chain} = \frac{1+u}{1-u}\chi_t \quad (1)$$

$$u = \coth(J_2 S_t(S_t+1)/kT) - kT/J_2 S_t(S_t+1) \quad (2)$$

$$\chi_t = \frac{Ng^2\beta^2}{3kT} S_t(S_t+1) \quad (3)$$

$$S_t(S_t+1) = \frac{3}{4} \times \frac{1+e^{2J_1/kT}+10e^{3J_1/kT}}{1+e^{2J_1/kT}+2e^{3J_1/kT}} \quad (4)$$

The best least-square fit of the experimental susceptibilities of **2** to the Eqs. (1)–(4) above 40.0 K leads to J_1 = –176 cm^{-1}, J_2 = – 0.9 cm^{-1}, g = 2.18 and $R = 1.5\times10^{-3}$. The J_1 describes the strength of the superexchange pathway involved in μ-OH^- and μ-N1, N2-atr mediators, because they located respectively at the square-planar positions of Cu1 and basal positions of Cu2. Moreover, the bigger bond angles of ∠Cu–N–N (121.394(2)º and 119.932(2)º) and ∠Cu–O–Cu (103.244(8)º) can further benefit the overlap between the magnetic orbits of the Cu^{II} ion and the σ-orbit of the atr and hydroxyl group to produce the strong antiferromagnetic interaction. The large negative value of J_1 is also comparable with the reported Cu^{II} complexes with the same heterobridges.[30-31] By contrast, the J_2 suggests the magnetic strength mediated by pairs of the single-atom carboxylate bridges suited at the axial positions of the neighboring Cu2 ions.

The isothermal M–H curve of **2** at 2.0 K (Fig. 5b) can be fitted to a Brillouin function with S = 1/2, g = 2.14 and $R = 4.2\times10^{-4}$, suggesting that strong intra-subunit antiferromagnetic coupling coexists with the weak inter-subunit magnetic exchange. The magnetization for each Cu^{II}_3 subunit of **2** reaches a magnetic saturation (1.06 $N\beta$) at 70 kOe, further confirming the paramagnetic S = 1/2 spin ground-state of **2** at low temperature.

Much different from **2**, the room-temperature $\chi_M T$ product for each Cu^{II}_3 subunit of **3** (1.06 cm^3 K mol^{-1}, Fig. 5a) is only slightly lower than the expected value for three isolated Cu^{II} ions with S = 1/2 and g = 2.0 (1.12 cm^3 K

mol^{-1}), suggesting a weak magnetic interaction of **3** than **2** at room temperature. The $\chi_M T$ value decreases moderately with the decreasing temperature and is down to 0.04 cm^3 K mol^{-1} at 2.0 K, indicating that the adjacent spin carriers in the chain are strongly antiferromagnetically coupled to each other to result in a diamagnetic $S = 0$ spin ground-state. The $S = 0$ spin ground-state of **3** at low temperature can be further evidenced by the linear M–H curve measured at 2.0 K with an unsaturated magnetization (0.22 $N\beta$ for Cu^{II}_3 subunit) at 70 kOe (Fig. 5b).

To quantitatively obtain the intra- and inter-subunit coupling constants by the mixed multiple heterobridges (μ-atr, μ-OH^-, μ-ClO_4^-, $\mu_{1,1,5,5}$-dca^- and μ-N1,N2-atr), the same magnetic mode as **2** is used to evaluate the magnetic data of **3**. The best least-square fit of the experimental magnetic data of **3** to the Eqs (1)–(4) gives rise to $g = 2.14$, $J_1 = -43$ cm^{-1}, $J_2 = -127$ cm^{-1} and $R = 4.7\times10^{-4}$. Obviously, two negative values for both J_1 and J_2 confirm the antiparallel arrangement of the magnetic moments between the adjacent Cu^{II} ions. The inter-subunit antiferromagnetic coupling by the four-fold heterobridges is stronger than that observed within the Cu^{II}_3 subunit by a pair of μ-N1,N2-atr and single atomic bridging CN^- mediators, which is just opposite to those of **2** and is in a good agreement with the established magnetostructural relationships. The relatively weak coupling of J_1 is due to the poor overlap between the $d(x^2$-$y^2)$ orbit of Cu^{II} ion and the σ orbit of atr ligand,[31] because the dihedral angles between the equatorial plane of the octahedral Cu^{II} ion and the atr ligand are 56.557(1)º and 56.955(3)º (for Cu1), 56.745(3)º and 48.121(3)º (for Cu2). By contrast, the inter-subunit Cu1 and mirror-symmetry Cu1A ions involving planes are almost coplanar with a dihedral angle of 8.026(4)º, which can produce good magnetic orbital overlap to give a strong inter-subunit antiferromagnetic coupling for J_2. Moreover, the significant contribution for the strong inter-subunit antiferromagnetic interaction is mainly from the mixed μ-OH^- and μ-N1,N2-atr mediators, because the axial ClO_4^- and dca^- bridges contribute little for the magnetic coupling.

/insert Figure 6/

Complex **4** features a field-induced metamagnetic transition from antiferromagnetic ordering to weak

ferromagnetic state. As illustrated in Fig. 6, the room-temperature $\chi_M T$ value for per Cu^{II}_3 subunit of **4** is 0.66 cm^3 K mol^{-1}, lower than the spin-only value for three magnetically uncoupled Cu^{II} ions with S = 1/2 and g = 2.0 (1.12 cm^3 K mol^{-1}). The $\chi_M T$ product decreases with the decreasing temperature and reaches to a value of 0.52 cm^3 K mol^{-1} at 75.0 K. Then, it rises to a sharp maximum of 0.66 cm^3 K mol^{-1} at 6.0 K and finally drops due to the interlayer antiferromagnetic interactions. The sudden increase of $\chi_M T$ at low temperature implies weak spontaneous magnetization of **4** probably due to the inter-subunit ferromagnetic interactions. To exactly evaluate the significant magnetic interactions associated with the Cu^{II}_3-based 1D chain, the same magnetic model as **2** and **4** were applied to treat the magnetic data, in which the molecule-field approximation was introduced to estimate the weak interchain magnetic interactions by axial μ_3-OH^- and/or long spa^{3-} pillars. The magnetic fit of **4** was performed above 40.0 K and the resulting parameters are g = 2.16, J_1 = –173 cm^{-1}, J_2 = 47.2 cm^{-1}, zJ' = –3.2 cm^{-1} and $R = 9.5\times10^{-4}$. The J_1 value reveals the strong intra-subunit antiferromagnetic interactions by μ-N1,N2-atr and μ-OH^- heterobridges and the moderately positive J_2 indicates the moderate ferromagnetic interactions by μ-*syn*, *syn*-COO^- and μ_3-OH^- groups. The coupling strength mediated by the different pairs of heterobridges are comparable to those in **1**. The χ_M *vs.* T curves display a maximum around 2.0 K under the field lower than 7 kOe, suggesting an antiferromagnetic ordering of **4** at low external field. Moreover, the maximum of χ_M at low temperature becomes field-dependent and vanishes under high field, indicating a field-dependent metamagnetic transition.

The field-dependent magnetization of **4** measured at 2.0 K reveals a sigmoid-shaped increase with the increasing external fields (Fig. 5b), strongly suggesting the metamagnetic behavior of **4** with a critical field of *ca* 9 kOe determined by the dM/dH curve (Fig. S10 in the ESI†). The weak interchain or interlayer antiferromagnetic interaction by long spa^{3-} connectors and/or axial μ-OH^- group is overwhelmed by the strong external field to generate the metamagnetism of **4**. The magnetization of **4** at the highest field (0.95 $N\beta$) is consistent with that of

ferrimagnetic $S = 1/2$ spin ground-state.

Conclusion

By changing carboxylate-/cyanide-modified magnetic mediators, four linear Cu^{II}_3 subunit-based coordination polymers consisting of three bent 1D chains and one pillared-layer 3D framework were obtained. Crystallographically, these complexes exhibit various μ-N1,N2-atr-involved linear Cu^{II}_3 subunits and diverse inter-subunit connections arising from the cooperative binding of short multiple heterobridges towards the metal ions. Magnetically, different inter-/intra-subunit superexchange couplings lead to ferrimagnetic $S = 1/2$ (for **1** and **4**), paramagnetic $S = 1/2$ (for **2**) as well as diamagnetic $S = 0$ (for **3**) spin ground-states at low temperature. Furthermore, 3D framework of **4** exhibit metamagnetic behavior resulting from the competitive magnetic interactions between the interchain/interlayer antiferromagnetic coupling and the external magnetic field. These interesting results are significantly important and instructive for the design and preparation of the new cyclic polyazolate-based magnetic materials.

Acknowledgements

This present work was financially supported by the 973 Program (2014CB845601), the National Natural Science Foundation of China (Grants 21171129, 21173157, 21371134 and 21303121), Tianjin Municipal Education Commission (2012ZD02) and the Program for Innovative Research Team in University of Tianjin (TD12–5038), which are gratefully acknowledged.

References

1 M. Kurmoo, *Chem. Soc. Rev.*, 2009, **38**, 1353.

2 (*a*) E. Coronado and K. R. Dunbar, *Inorg. Chem.*, 2009, **48**, 5047; (*b*) D. Gatteschi, R. Sessoli, and R. Villain, *Molecular Nanomagnets*, Oxford University Press, Oxford, 2006.

3 (*a*) J. Lehmann, A. Gaita-Ariño, E. Coronadoc and D. Loss, *J. Mater. Chem.*, 2009, **19**, 1672; (*b*) C. Utfeld, S. R. Giblin, J. W. Taylor, J. A. Duffy, C. Shenton-Taylor, J. Laverock, S. B. Dugdale, M. Manno, C. Leighton, M. Itou, and Y. Sakurai, *Phys. Rev. Lett.*, 2009, **103**, 226403; (*c*) L. Bogani1 and W. Wernsdorfer, *Nat. Mater.*,

2008, **7**, 179.

4 J. Camarero and E. Coronado, *J. Mater. Chem.*, 2009, **19**, 1678.

5 Y.-F. Zeng, X. Hu, F.-C. Liu and X.-H. Bu, *Chem. Soc. Rev.*, 2009, **38**, 469.

6 X.-Y. Wang, Z.-M. Wang and S. Gao, *Chem. Commun.*, 2008, 281.

7 M. Dey and N. Gogoi, *Angew. Chem., Int. Ed.*, 2013, **52**, 12780.

8 A. Adhikary, J. A. Sheikh, S. Biswas and S. Konar, *Dalton Trans.*, 2014, **43**, 9334.

9 R. W. Hogue, R. G. Miller, N. G. White, H. L. C. Feltham, G. N. L. Jameson and S. Brooker, *Chem. Commun.*, 2014, **50**, 1435.

10 W. Ouellette, S. Jones and J. Zubieta, *CrystEngComm*, 2011, **13**, 4457.

11 E.-C. Yang, Y.-Y. Zhang, Z.-Y. Liu, X.-J. Zhao, *Inorg. Chem.*, 2014, **53**, 327.

12 J.-R. Li, Q. Yu, E. C. Sañudo, Y. Tao and X.-H. Bu, *Chem. Commun*., 2007, 2602.

13 X.-B. Li, G.-M. Zhuang, X. Wang, K. Wang and E.-Q. Gao, *Chem. Commun.*, 2013, **49**, 1814.

14 E.-C. Yang, Z.-Y. Liu, X.-Y. Wu and X.-J. Zhao, *Chem. Commun.*, 2011, **47**, 8629.

15 W. Ouellette, A. V. Prosvirin, V. Chieffo, K. R. Dunbar, B. Hudson, and J. Zubieta, *Inorg. Chem.*, 2006, **45**, 9346.

16 W. Ouellette, A. V. Prosvirin, K. Whitenack, K. R. Dunbar, J. Zubieta, *Angew. Chem., Int. Ed*., 2009, **48**, 2140.

17 G. M. Sheldrick, *SADABS*, University of Göttingen, Göttingen, Germany, 1996.

18 Bruker AXS, *SAINT software Reference Manual*, Madison, WI, 1998.

19 (*a*) G. M. Sheldrick, *SHELXL-97, Program for X-ray Crystal Structure Refinement*, Göttingen University, Göttingen, Germany, 1997; (*b*) G. M. Sheldrick, *SHELXS-97, Program for X-ray Crystal Structure Solution*, Göttingen University, Göttingen, Germany, 1997.

20 K. Nakamoto, *Infrared and Roman Spectra of Inorganic and Coordination Compounds*, Wiley, New York, 1986.

21 A. W. Addison, T. N. Rao, J. Reedijk, J. V. Rijn and G. C. Verschoor, *J. Chem. Soc., Dalton Trans.*, 1984, 1349.

22 E.-C. Yang, B. Ding, Z.-Y. Liu, Y.-L. Yang and X.-J. Zhao, *Cryst. Growth Des*., 2012, **12**, 1185.

23 M. S. E. Fallah, R. Vicente, J. Tercero, C. Elpelt, E. Rentschler, X. Solans and M. Font-Bardia, *Inorg. Chem*., 2008, **47**, 6322.

24 (*a*) J. J. Borrás-Almenar, J. M. Clemente-Juan, E. Coronado and B. S. Tsukerblat, *Inorg. Chem*., 1999, **38**, 6081; (*b*) J. J. Borrás-Almenar, J. M. Clemente-Juan, E. Coronado and B. S. Tsukerblat, *J. Comput. Chem*.,

2001, **22**, 985.

25 E.-C. Yang, X.-G Wang, C.-H. Zhang, N. Yang, Z.-Y. Liu, X.-J. Zhao, *Sci. China Chem.*, 2013, **56**, 465.

26 (*a*) L. K. Thompson, S. S. Tandon, F. Lloret, J. Cano and M. Julve, *Inorg. Chem*., 1997, **36**, 3301; (*b*) L.-L. Wang, Y.-M. Sun, Z.-N. Qi and C.-B. Liu, *J. Phsy. Chem. A*, 2008, **112**, 8418.

27 H.-Z. Kou, B.-C. Zhou, D.-Z. Liao, R.-J. Wang, Y.-D. Li, *Inorg. Chem*., 2002, **41**, 6887.

28 Y.-F. Yang, Y.-S. Ma, L.-R. Guo, L.-M. Zheng, *Cryst. Growth. Des.*, 2008, **8**, 1213.

29 O. Kahn, *Molecular Magnetism*, Wiley-VCH, Weinheim, 1993.

30 (*a*) J.-H. Zhou, R.-M. Cheng, Y. Song, Y.-Z. Li, X.-T. Chen, Z.-L. Xue and X.-Z. You, *Inorg. Chem*., 2005, **44**, 8011; (*b*) E.-C. Yang, Z.-Y. Liu, C.-H. Zhang, Y.-L. Yang and X.-J. Zhao, *Dalton Trans*., 2013, **42**, 1581; (*c*) E.-C. Yang, B. Ding, Z.-Y. Liu, Y.-L. Yang and X.-J. Zhao, *Cryst. Growth Des*., 2012, **12**, 1185

31 Z.-Y. Liu, Y.-H. Su, E.-C. Yang and X.-J. Zhao, *Inorg. Chem. Commun.*, 2012, **26**, 56.

Table 1 Crystal data and structure refinement for **1**–**4**

	1	**2**	**3**	**4**
Chemical formula	$Cu_2C_{10}H_{14}N_4O_8$	$Cu_{1.5}C_{10}H_{12}N_5O_9$	$C_{12}H_{21}N_{23}O_{17}Cl_4Cu_3$	$C_{24}H_{38}Cu_6N_{16}O_{25}S_2$
fw	445.33	441.56	1091.94	1396.06
Crystal sys	triclinic	triclinic	orthorhombic	monoclinic
Space group	$P\bar{1}$	$P\bar{1}$	*Pnma*	*C*2/*c*
a / Å	7.033(2)	7.5559(5)	12.2905(17)	23.989(6)
b / Å	10.495(4)	9.5691(7)	17.329(2)	15.168(4)
c / Å	10.724(3)	10.5354(7)	17.319(2)	14.285(4)
α / °	108.425(4)	102.7580(10)	90	90
β / °	92.075(4)	97.5380(10)	90	119.389(4)
γ / °	102.894(4)	93.1230(10)	90	90
V / Å^3	727.2(4)	733.77(9)	3688.6(8)	4528.9(19)
Z	2	2	4	4
ρ / mg m^{-3}	2.034	1.999	1.966	2.047
μ / mm^{-1}	2.977	2.258	2.104	2.965
Data / restraints / params	2543 / 1 / 220	2570 / 46 / 246	3376 / 101 / 299	3968 / 0 / 343
R_{int}	0.0148	0.0133	0.0673	0.0385
R_1[a], wR_2[b] ($I > 2\sigma(I)$)	0.0419, 0.1017	0.0392, 0.0956	0.0720 / 0.1772	0.0414 / 0.0953
R_1, wR_2 (all data)	0.0566, 0.1094	0.0450, 0.0998	0.0965 / 0.1921	0.0665 / 0.1080
ρ_{max}, ρ_{min} /e·Å^{-3}	0.770, −0.944	1.185, −0.853	1.778, – 0.938	0.981, – 0.546

[a] $R_1 = \Sigma(||F_o|-|F_c||)/\Sigma|F_o|$. [b] $wR_2 = [\Sigma w(|F_o|^2-|F_c|^2)^2/\Sigma w(F_o^2)^2]^{1/2}$.

Captions to Figures

Fig. 1 (a) Local coordination environments of the Cu^{II} ions in **1**. H atoms were omitted for clarity, symmetry codes: A = – *x*, 1 – *y*, 2 – *z*; B = – *x*, – *y*, 1 – *z*. Selected bond lengths (Å): Cu1–O7W 2.341(5), Cu1–O5 1.928(3), Cu1–N1 2.009(4), Cu1–O6 1.911(4), Cu1–O2 1.969(3), Cu2–O6 1.880(3), Cu2–N2 1.986(4), Cu3–O1 1.973(3), Cu3–O5 1.892(3). (b) Bent chain of **1** with two linear Cu^{II}_3 subunits alternately connected by sharing the same vertex.

Fig. 2 (a) Local coordination environments of the Cu^{II} ions in **2**. H atoms were omitted for clarity, symmetry codes: A = – *x*, 1 – *y*, 1 – *z*; B = – *x*, 2 – *y*, 1 – *z*. Selected bond lengths (Å): Cu2–O3 2.361(3), Cu2–O3B 2.000(3), Cu2–O8 1.910(3), Cu2–O7 1.931(3). (b) Linear Cu^{II}_3 core-based *zigzag* chain of **2** extended by carboxylate of npa^{2-} connectors.

Fig. 3 (a) Local coordination environments of the Cu^{II} ions in **3**. H atoms were omitted for clarity, symmetry codes: A = – *x*, – *y*, 1 – *z*; B = *x*, 0.5 – *y*, *z*. Selected bond lengths (Å): Cu1–N12 2.557(7), Cu1–O6 2.553(7), Cu1–O1 1.871(4), Cu1–N9 2.006(7), Cu1–N6 1.990(7), Cu1–N2 1.988(7), Cu2–N12 2.362(8). (b) Linear Cu^{II}_3 core-based bent chain of **3** extended by mixed four-fold connectors.

Fig. 4 (a) Local coordination environments of the Cu^{II} ions in **4**. H atoms were omitted for clarity, symmetry codes: A = 0.5 – *x*, 0.5 + *y*, 0.5 – *z*; B = 0.5– *x*, 0.5 – *y*, 1 – *z*; C = 1 – *x*, *y*, 1.5 – *z*. Selected bond lengths (Å): Cu1–O8B 2.492(5), Cu2–O5C 2.597(8), Cu3–O11 2.381(5). (b) 2D layer of **4** constructed from Cu^{II}_3-based chains and pairs of μ_3-OH^- groups. (c) Pillar-layered framework of **4**.

Fig. 5 (a) Temperature dependence of $\chi_M T$ for **1–3**. The solid lines represent the best fits indicated in the text (Inset: spin arrangement in the Cu^{II}_3 subunit-based 1D chain). (b) Field dependence of magnetization for **1–4** measured at 2.0 K.

Fig. 6 Temperature dependence of $\chi_M T$ for **4** under different applied fields and the spin alignment in the local 1D chain. The solid line represents the best fit indicated in the text.

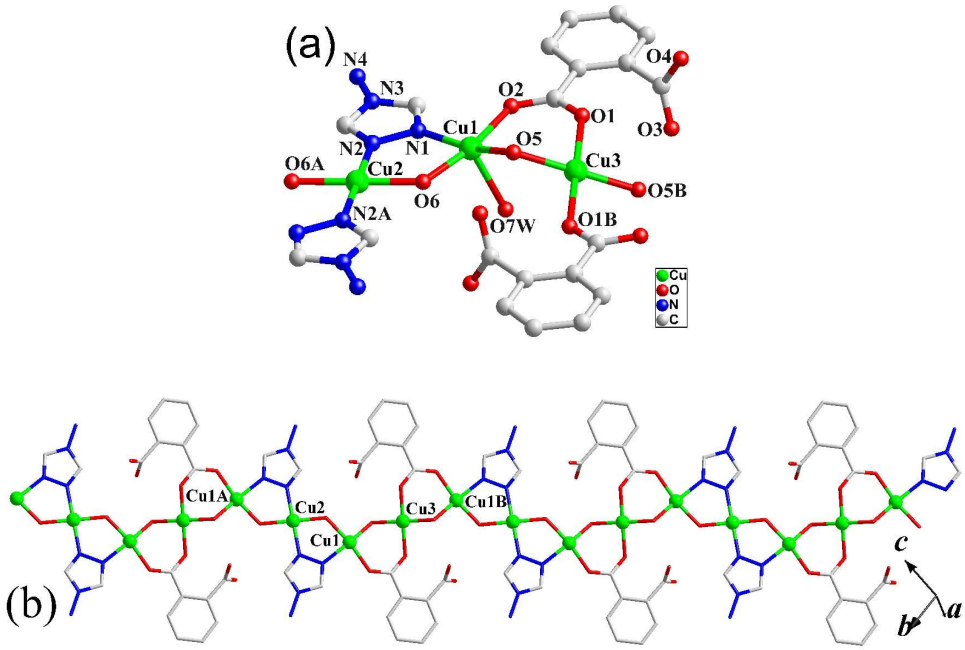

Fig. 1

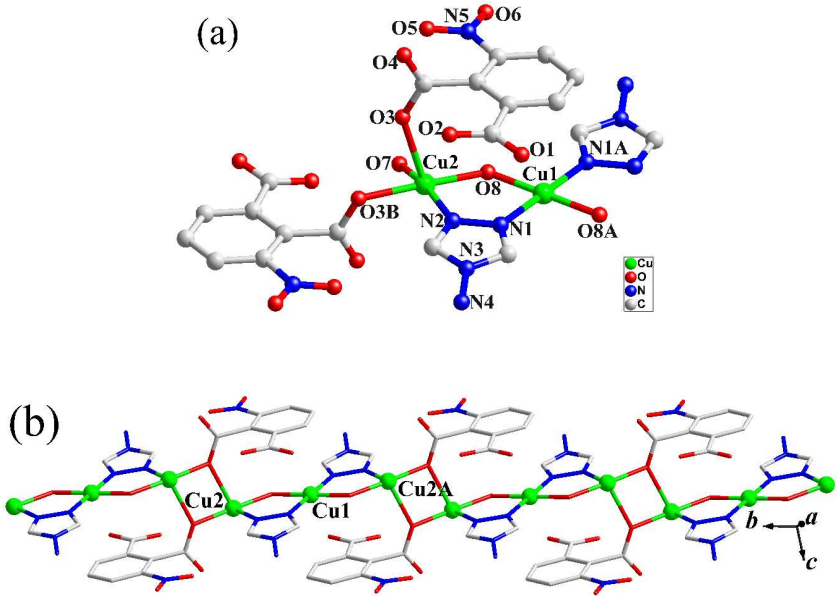

Fig. 2

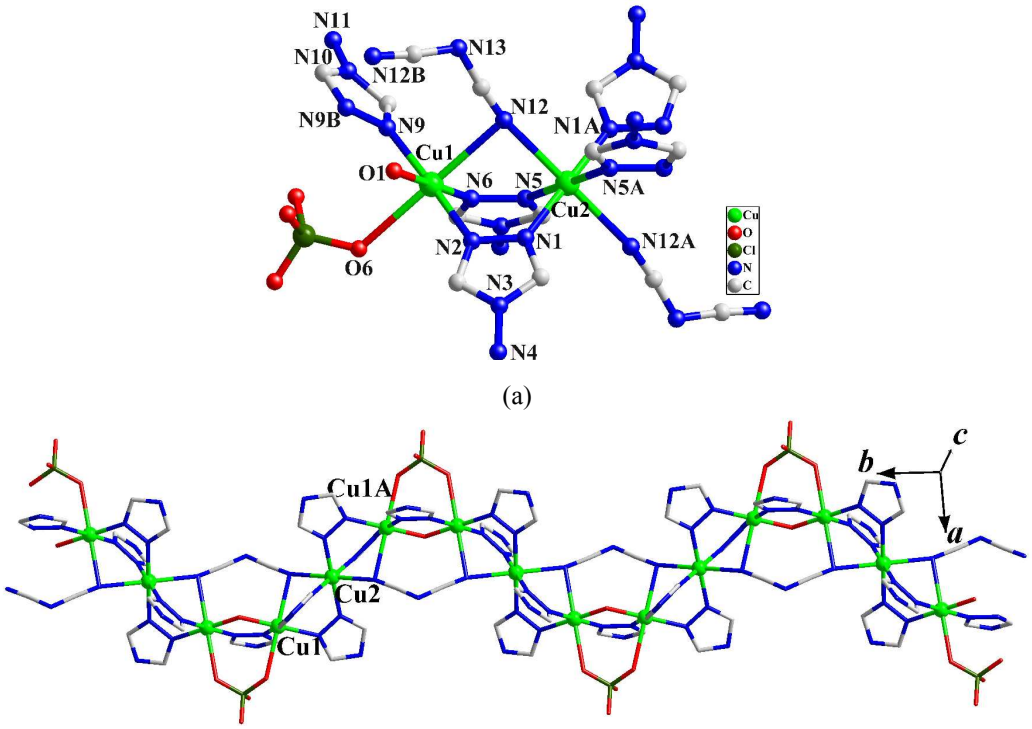

Fig. 3

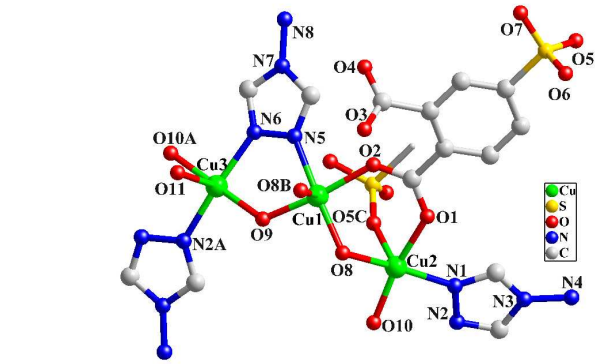

(a)

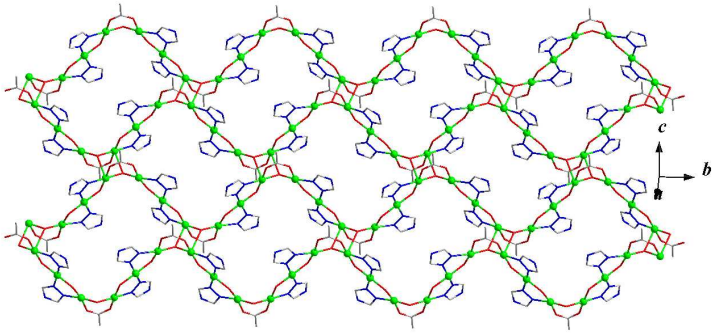

(b)

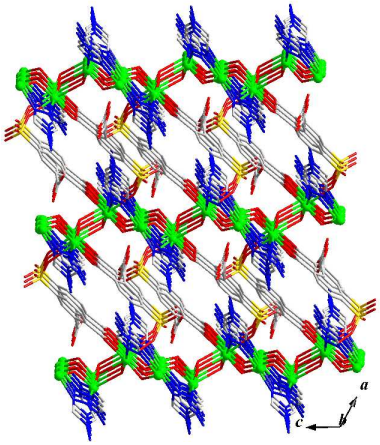

(c)

Fig. 4

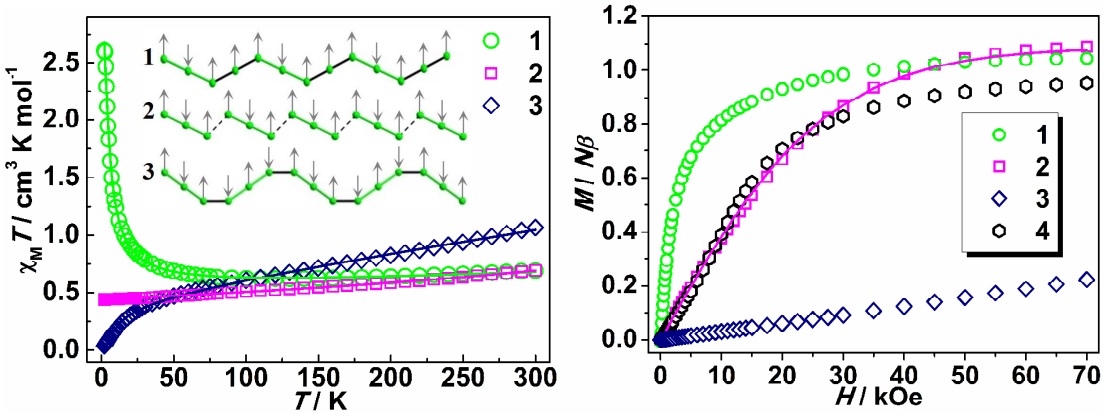

(a) (b)

Fig. 5

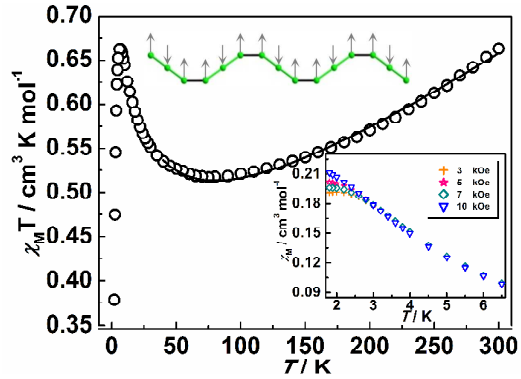

Fig. 6

Contents entry

Four linear Cu^{II}_3 subunit-based coordination polymers with various inter-subunit connections, spin ground-states and intra-/inter-subunit magnetic couplings

En-Cui Yang,[a *] Zhong-Yi Liu,[a] Si-Hang Chen,[a] Yan-Hong Su,[a] Yan-Yan Zhang[a] and Xiao-Jun Zhao[a, b *]

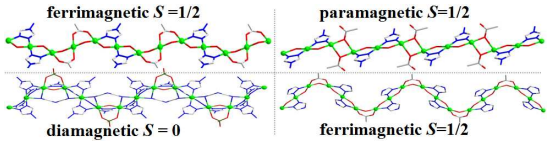

Four 4-amino-1,2,4-triazole-based complexes including three bent chains and one pillared-layer framework were reported, which exhibit various linear Cu^{II}_3 subunits, inter-subunit connections, spin ground-states and magnetic couplings.